Homozygous loss of autism-risk gene *CNTNAP2* results in reduced local and long-range prefrontal functional connectivity

Adam Liska[1,2] MSc

Ryszard Gomolka[1] MSc,

Mara Sabbioni[3] Msc,

Alberto Galbusera[1] MSc

Stefano Panzeri[4] PhD

Maria Luisa Scattoni[3] PhD

Alessandro Gozzi[1]* PhD

[1]Functional Neuroimaging Laboratory, Istituto Italiano di Tecnologia, Center for Neuroscience and Cognitive Systems @ UniTn, 38068, Rovereto, ITALY

[2]CIMEC, Center for Mind/Brain Sciences, University of Trento, Rovereto, Italy

[3] Istituto Superiore di Sanità, Neurotoxicology and Neuroendocrinology Section, Department of Cell Biology and Neurosciences, Rome, ITALY

[4] Neural Computation Laboratory, Istituto Italiano di Tecnologia, Center for Neuroscience and Cognitive Systems @ UniTn, 38068, Rovereto, ITALY

Corresponding author:
Alessandro Gozzi
Functional Neuroimaging Laboratory, Istituto Italiano di Tecnologia, Center for Neuroscience and Cognitive Systems @uniTn,
38068, Rovereto, ITALY

Tel +39 335 353 830
alessandro.gozzi@iit.it

Abbreviated title: Reduced connectivity in CNTNAP2-null mice

Keywords: fMRI, CASPR2, DMN, mouse, ASD

Abstract

Functional connectivity aberrancies, as measured with resting-state fMRI (rsfMRI), have been consistently observed in the brain of autism spectrum disorders (ASD) patients. However, the genetic and neurobiological underpinnings of these findings remain unclear. Homozygous mutations in *Contactin Associated Protein-like 2* (*CNTNAP2*), a neurexin-related cell-adhesion molecule, are strongly linked to autism and epilepsy. Here we used high field rsfMRI to show that homozygous mice lacking *CNTNAP2* exhibit reduced long-range and local functional connectivity in prefrontal and midline "functional hubs" of the mouse brain. Long-range rsfMRI connectivity impairments affected heteromodal cortical regions and were prominent between frontal and posterior components of the mouse default mode network (DMN), an effect that was associated with reduced social investigation, a core "autism trait" in mice. We did not observe genotype-dependent differences in cortico-cortical white matter connectivity as measured with MRI-based fibre tractography, thus supporting a functional origin for the observed rsfMRI desynchronization. These findings reveal a key contribution of ASD-associated gene CNTNAP2 in modulating macroscale functional connectivity, and suggest that homozygous loss-of-function mutations in this gene may predispose to neurodevelopmental disorders and autism through a selective dysregulation of functional coupling between integrative heteromodal cortical areas.

Introduction

Neuroimaging and postmortem studies have consistently revealed impaired or atypical functional connectivity across brain regions of autistic spectrum disorders (ASD) patients (Anagnostou and Taylor, 2011). These findings have led to the hypothesis that aberrant connectivity patterns might represent a common final pathway or neurobiological pathogenetic correlate of the autistic phenotype to which different ASD etiologies may converge (Just et al., 2012). Although great heterogeneity exists in the sign and distribution of abnormal connectivity across studies and imaging modalities, consistent features indeed appear to emerge, including reduced functional coherence of long-range intra-hemispheric cortico-cortical default mode circuitry, impaired inter-hemispheric regulation and possibly increase in local and short-range cortico-subcortical coherence (Rane et al., 2015). However, the neurophysiological underpinnings of these connectional derangements are largely unknown, and a causal etiopathological contribution of specific genetic variants to impaired connectivity in ASD remains to be firmly established.

Mouse lines recapitulating high-confidence ASD mutations (Sanders et al., 2015) have been employed to understand how specific genetic alterations translate into relevant changes in cells and circuits (Auerbach et al., 2011). The recent optimization of neuroimaging readouts of functional connectivity such as resting-state functional MRI (rsfMRI) in the mouse (Sforazzini et al., 2014b) permits to extend this paradigm to the investigation of the elusive genetic and neurobiological foundations of aberrant connectivity observed in ASD (Sforazzini et al., 2014a). The approach leverages on the identification of robust homotopic and distributed rsfMRI

connectivity networks in the mouse, including possible homologues of distributed human rsfMRI systems like the salience and default mode (DMN) networks (Gozzi and Schwarz, 2015), and the observation that cyto-architecturally conserved heteromodal cortices in cingulate and retrosplenial regions exhibit similar "hub-like" topological properties in both species (Liska et al., 2015;Cole et al., 2010). Importantly, as mouse rsfMRI measurements rest on the same biophysical principles of corresponding human neuroimaging readouts, this approach has the merit of providing a direct translational bridge across species.

Homozygous loss-of-function mutations in *Contactin Associated Protein-like 2* (*CNTNAP2*) encoding CASPR2, a neurexin-related cell-adhesion molecule, are strongly linked to autism and epilepsy in consanguineous families (Alarcin et al., 2008;Rodenas-Cuadrado et al., 2014;Strauss et al., 2006). Loss of CNTNAP2 in mice leads to abnormal neuronal migration, reduced GABAergic neurons, spontaneous seizures, and behavioural traits consistent with ASD symptoms in humans (Penagarikano et al., 2011), an ensemble of traits that phenocopy major neuropathological features observed in cortical dysplasia-focal epilepsy (CDFE) syndrome, a rare neuronal migration disorder associated with a recessive mutation in CNTNAP2 (Strauss et al., 2006). Interestingly, common genetic variants in CNTNAP2 were recently described to be associated with impaired frontal lobe connectivity in humans (Scott-Van Zeeland et al., 2010). However, a causal relationship between ASD-related loss-of-function mutations in CNTNAP2 and functional connectivity remains to be firmly established. Moreover, the role of CNTNAP2 in shaping macroscale circuit assembly, and the specific substrates affected, remain largely unknown.

To address these questions, we used BOLD rsfMRI and diffusion-weighted MRI to map large-scale functional connectivity and white matter topology in homozygous CNTNAP2-null mice (*Cntnap2*$^{-/-}$). We document that loss of CNTNAP2 results in local and long-range connectivity reductions affecting prefrontal regions that act as "functional connectivity hubs" in the mouse brain (Liska et al., 2015). We also show that fronto-posterior *hypo-connectivity* is associated with impaired social behaviour. A lack of connectional alterations at the macroscale suggests that the observed functional connectivity abnormalities reflect functional decoupling, rather than major white matter re-wiring. Collectively, these findings reveal a role of autism-risk gene CNTNAP2 in modulating functional network assembly between key integrative connectivity hubs of the mammalian brain. The observed long-range prefrontal hypo-connectivity in *Cntnap2*$^{-/-}$ mice recapitulates imaging findings in autism and adds to the construct validity of this mouse line to model ASD-related phenotypes.

Materials and Methods

Ethical Statement

All in vivo studies were conducted in accordance with the Italian law (DL 116, 1992 Ministero della Sanità, Roma) and the recommendations in the Guide for the Care and Use of Laboratory Animals of the National Institutes of Health. Animal research protocols were also reviewed and consented to by the animal care committee of the Istituto Italiano di Tecnologia. The Italian Ministry of Health specifically approved the protocol of this study, authorization n° 07753 to A.G. All surgical procedures were performed under anaesthesia.

Social interaction

CNTNAP2-null (Cntnap2$^{-/-}$) and control "wild-type" (Cntnap2$^{+/+}$) breeding pairs were obtained from Jackson Laboratories (Bar Harbor, ME, USA) and bred locally. Mice were housed by sex in mixed genotype groups, with temperature maintained at 21 ± 1°C and humidity at 60 ± 10%. Three-month-old male mice (N=13 *Cntnap2*$^{+/+}$; N=13 *Cntnap2*$^{-/-}$) were evaluated in the male–female social interaction test during the light phase, as previously described (Scattoni et al., 2011;Scattoni et al., 2013). An unfamiliar stimulus control female mouse in estrous was placed into the home-cage of an isolated test male mouse, and social behaviour plus ultrasonic vocalizations (USVs) were recorded during a 3-min test session. Scoring of social investigation parameters was conducted using Noldus Observer 10XT software (Noldus Information Technology, Leesburg, VA, USA). Social interactions were defined as number of events (frequency) and duration of the following behavioural responses performed by the test mouse: anogenital sniffing (direct contact with the anogenital area), body sniffing (sniffing or snout

contact with the flank area), head sniffing (sniffing or snout contact with the head/neck/mouth area), locomotor activity, rearing up against the wall of the home-cage, digging in the bedding, and grooming (self-cleaning, licking any part of its own body). No observations of mounting, fighting, tail rattling, and wrestling behaviours were observed. Scoring was rated by two investigators blind to genotype. Inter-rater reliability was 98%. To measure ultrasound vocalization recordings, an ultrasonic microphone (Avisoft UltraSoundGate condenser microphone capsule CM16, Avisoft Bioacoustics, Berlin, Germany) was mounted 20 cm above the cage and the USVs recorded using Avisoft RECORDER software version 3.2. Settings included sampling rate at 250 kHz; format 16 bit. The ultrasonic microphone was sensitive to frequencies between 10 and 180 kHz. For acoustical analysis, recordings were transferred to Avisoft SASLabPro (version 4.40) and a fast Fourier transformation (FFT) was conducted as previously described (Scattoni et al., 2008). Start times for the video and audio files were synchronized.

Resting state fMRI

rsfMRI experiments were performed on the same experimental cohorts employed in the behavioural tests (N=13 Cntnap2$^{+/+}$; N=13 Cntnap2$^{-/-}$). The animal preparation protocol was recently described in great detail (Ferrari et al., 2012;Sforazzini et al., 2014a). Briefly, mice were anaesthetized with isoflurane (5% induction), intubated and artificially ventilated (2% maintenance). The left femoral artery was cannulated for continuous blood pressure monitoring and terminal arterial blood sampling. At the end of surgery, isoflurane was discontinued and substituted with halothane (0.75%). Functional data acquisition commenced 45 min after isoflurane cessation. Mean arterial blood pressure was recorded throughout the imaging sessions. Arterial blood gases (p_aCO_2 and p_aO_2) were measured at the end of the functional time

series to exclude non-physiological conditions. Mean p_aCO_2 and p_aO_2 levels recorded were 17±3 and 250±29 mmHg in *Cntnap2*$^{+/+}$ and 15±3 and 231±38 mmHg in *Cntnap2*$^{-/-}$. Possible genotype-dependent differences in anaesthesia sensitivity were evaluated using Student's two-sample *t*-test applied to two independent readouts previously shown to be linearly correlated with anaesthesia depth: mean arterial blood pressure and amplitude of cortical BOLD signal fluctuations (Steffey et al., 2003;Liu et al., 2011;Zhan et al., 2014).

rsfMRI images were acquired with a 7.0 Tesla MRI scanner (Bruker Biospin, Milan) as previously described (Liska et al., 2015), using a 72 mm birdcage transmit coil, and a four-channel solenoid coil for signal reception. For each session, high-resolution anatomical images were acquired with a fast spin echo sequence (repetition time (TR)/echo time (TE) 5500/60 ms, matrix 192 × 192, field of view 2 × 2 cm^2, 24 coronal slices, slice thickness 0.50 mm). Co-centred single-shot BOLD rsfMRI time series were acquired using an echo planar imaging sequence with the following parameters: TR/TE 1200/15 ms, flip angle 30°, matrix 100 × 100, field of view 2 × 2 cm^2, 24 coronal slices, slice thickness 0.50 mm, 500 volumes and a total rsfMRI acquisition time of 10 min.

Functional connectivity analyses

The first 20 volumes of the rsfMRI data were removed to allow for T1 equilibration effects. The time series were then despiked, corrected for motion and spatially normalized to an in-house mouse brain template (Sforazzini et al., 2014b). The normalised data had a spatial resolution of 0.1042 × 0.1042 × 0.5 mm^3 (192 × 192 × 24 matrix). Head motion traces and mean ventricular signal (averaged rsfMRI time course within a reference ventricular mask) were regressed out of

each of the time series. No inter-group differences in ventricular volume was observed as measured by the dimension of individual ventricular masks (p=0.31). All rsfMRI time series were spatially smoothed (full width at half maximum of 0.6 mm) and band-pass filtered to a frequency window of 0.01-0.1 Hz.

To obtain an unbiased identification of the brain regions exhibiting genotype-dependent differences in functional connectivity, we employed the global brain connectivity (GBC) method (Liska et al., 2015;Cole et al.,) and calculated GBC maps for all subjects. This metric considers connectivity of a given voxel to all other voxels simultaneously by computing average connectivity strength. Specifically, we employed the weighted GBC method, in which individual *r*-scores are first transformed to *z*-scores using Fisher's *r*-to-*z* transform and then averaged to yield the final GBC voxel value. Local connectivity strength was mapped by limiting this measurement to connections within a 0.6252 mm sphere around each voxel (6 voxels in plane), while long-range connectivity was computed by considering only connections to voxels outside this sphere. Voxelwise inter-group differences in each of these parameters were mapped using a Student's *t*-test ($t(24) = 2.06$, $p < 0.05$ followed by a cluster correction with $p_c < 0.05$ as implemented in FSL). The effect was also quantified in volumes of interest (VOIs). The anatomical location of the examined VOIs is reported in Figure S1. Region identification and naming follow classic neuroanatomical labelling described in (Paxinos and Franklin, 2003). Many of these regions have recently been reclassified according to their cytoarchitectural properties such to match analogous regions in human and primates (Vogt and Paxinos, 2014). According to this scheme, the mouse prelimbic cortex corresponds to Brodmann Area 32 (A32), Cingulate cortex area 1

(anteriro cingulate cortex) to Brodmann area A24b, infralimbic cortex to A24a, retrosplenial cortex to areas A30 and A29.

Inter-group differences in the extension and intensity of long-range rsfMRI correlation networks were mapped using seed-based approach as previously described (Sforazzini et al., 2014a). Small *a priori* seed regions of 3×3×1 voxels were chosen to cover antero-posterior cortical networks, and representative heteromodal cortical structures. The seed locations and names are reported in Figure S2. The mean time courses from the unilateral (medial) and bilateral seeds (TeA, Pt, and vHC) were used as regressors for each voxel. Group level differences in connectivity distributions were mapped using two-sample Student's *t*-tests ($t(24) = 2.06$, $p < 0.05$, cluster correction with $p_c < 0.05$). Alterations in inter-hemispheric functional connectivity were assessed by computing correlation coefficients of inter-hemispheric VOI pairs depicted in Figure S1. The statistical significance of inter-group correlation strength in each region was assessed with a Student's *t*-test, followed by multiple comparison correction using a false discovery rate $q = 0.05$ according to the Benjamini-Hochberg procedure. Anteroposterior DMN hypoconnectivity was mapped by computing seed-to-VOI correlations. Prelimbic and cingulate cortex were employed as pefrontal volumes of interest. The location of seeds employed for mapping are indicated in Figure S2. The statistical significance of inter-group effects was quantified using a 2-way ANOVA, where seed–location and genotype were used as variables.

Diffusion MRI

Ex vivo diffusion-weighted (DW) MRI was carried out on paraformaldehyde fixed specimens as previously described (Dodero et al., 2013). At the end of the rsfMRI experiments mice were

transcardially perfused with 4% para-formaldehyde under deep isoflurane anaesthesia. Brains were imaged inside intact skulls to avoid post-extraction deformations. Each DW dataset was composed of 8 non-diffusion-weighted images and 81 different diffusion gradient-encoding directions with b=3000 s/mm^2 (∂=6 ms, Δ=13 ms) acquired using an EPI sequence with the following parameters: TR/TE=13500/27.6 ms, field of view 1.68 × 1.54 cm^2, matrix 120 × 110 (in-plane spatial resolution 140 x 140 µm^2), slice thickness 280 µm in the coronal plane, number of averages 20. Three mice were discarded from the analyses owing to the presence of large susceptibility distortions in the DW images due to the presence of air bubbles following imperfect perfusion procedure. As a result of this, the final number of subjects per group was N=13 and N=10, for *Cntnap2*$^{+/+}$ and *Cntnap2*$^{-/-}$, respectively.

White-matter fibre tractography

The DW datasets were first corrected for eddy current distortions (FSL/eddy_correct) and skull-stripped (Oguz et al., 2014). The resulting individual brain masks were manually corrected using ITK-SNAP (Yushkevich et al., 2006). Whole brain tractography was performed using MRtrix3 (Tournier et al., 2012) using constrained spherical deconvolution (l_{max} = 8, (Tournier et al., 2007)) and probabilistic tracking (iFOD2, (Tournier et al., 2012)) with a FOD amplitude cut-off of 0.2. For each dataset, the whole brain mask was used as a seed, and a total of 100,000 streamlines were generated.

The corpus callosum and cingulum were selected as tracts of interest, given their major cortico-cortical extension and direct involvement in prefrontal-posterior connectivity (Vogt and Paxinos, 2014). The tracts were virtually dissected with waypoint VOIs described in Figure S3 using

TrackVis (http://www.trackvis.org/). Inter-group differences in streamline counts of the tracts were evaluated using a Student's *t*-test. To provide a visual assessment of fibre distribution across groups, voxelwise parametric fibre density maps were generated using DiPy (Garyfallidis et al., 2014), by determining for each voxel the number of subjects in which at least one streamline of the fibre tract of interest passes through the voxel. For visualization purposes, both the dissected tracts and group fibre density maps were transformed to the Allen Mouse Common Coordinate Framework, Version 3 (http://www.brain-map.org/).

Results

Reduced local and long-range connectivity in fronto-cortical regions of Cntnap2$^{-/-}$ mice

In humans, CNTNAP2 variants have been associated with alterations in both local and long-range connectivity (Scott-Van Zeeland et al., 2010). To obtain an unbiased mapping of genotype-dependent differences in local and long-range connectivity, we implemented recently-developed aggregative metrics for these parameters (Liska et al., 2015;Cole et al., 2010). This analysis revealed foci of significantly reduced local and long-range connectivity in *Cntnap2*$^{-/-}$ mutants with respect to wild-type control subjects ($p < 0.05$, cluster corrected, Fig. 1) encompassing prefrontal (prelimbic and cingulate) and retrosplenial cortices. These same brain regions have been classified both in mice and in humans as "high strength" functional connectivity hubs (Buckner et al., 2009;Cole et al., 2010;Liska et al., 2015), and as such are thought to play a key integrative contribution in distributed functional networks. The effect was statistically significant also when integrated over large volumes of interest (Fig. 1). Local connectivity reductions appeared to be larger and more prominent than corresponding foci of long-range hypo-connectivity.

Long-range connectivity impairments in Cntnap2$^{-/-}$ mice affect heteromodal cortical regions and the DMN

To identify regional targets of the observed long-range connectivity deficits, we probed rsfMRI networks previously shown to involve prefrontal, cingulate and retrosplenial regions (Sforazzini et al., 2014b;Gozzi and Schwarz, 2015) (Fig. 2). Seed-based mapping of retrosplenial and anterior cingulate / prelimbic cortex highlighted foci of reciprocal long-range hypoconnectivity along the

midline brain axis in *Cntnap2*$^{-/-}$ mutants. We also probed connectivity of putative lateral components of the of the rodent DMN such as the posterior parietal and temporal association/auditory cortices, and postero-ventral hippocampus (Gozzi and Schwarz, 2015). Parietal cortical mapping revealed foci of reduced local and long-range (middle cingulate) connectivity in *Cntnap2*$^{-/-}$ mice. In the same animals, temporal association areas appeared to be widely hypo-connected to retrosplenial, cingulate and prefrontal regions. We also observed foci of long-range hypo-connectivity between ventral hippocampal and ventral prefrontal (infralimbic) regions (Fig. 2). Inter-hemispheric connectivity in subcortical or motor-sensory networks appeared to be overall largely preserved. A reduction in inter-hemispheric connectivity was observed in primary motor areas and visual cortex when quantified in anatomical volumes of interest (Fig. S4), although the effect did not survive correction for multiple comparisons using a false discovery rate of q=0.05.

Importantly, no genotype-dependent differences in anaesthesia sensitivity were detected as seen with mean arterial blood pressure mapping (Fig. S5A, p=0.78) and amplitude of cortical BOLD signal fluctuations (Fig. S5B, p=0.36), two independent readouts previously shown to be linearly correlated with anaesthesia depth (Steffey et al., 2003;Liu et al., 2011). Together with the observation of region-dependent alterations (as opposed to the global reduction described with increased anaesthesia dosing (Nasrallah et al., 2014)), these findings strongly argue against a confounding contribution of anaesthesia to the observed hypo-connectivity.

Hypo-connectivity in the mouse DMN is associated with impaired social behaviour

Recent human imaging studies in socially-impaired patients have revealed a putative association between long-range DMN hypo-connectivity and social competence (Schreiner et al., 2014). Based on these findings, we hypothesized that reduced long-range DMN connectivity in *Cntnap2*$^{-/-}$ mice could be associated with impaired social behaviour. To test this hypothesis, we first corroborated DMN hypoconnectivity by quantifying functional connectivity along the dorsal midline axis of this network (anterior, middle cingulate cortex, and retrosplenial cortex) using multiple seed-to-VOI measurements (Fig. 3). A clear dysconnection between posterior (retrosplenial) and middle/anterior portions of the DMN (cingulate, prelimbic cortex) was apparent (Fig. 3, retrosplenial vs. cingulate cortex p=0.025; retrosplenial-cingulate to prelimbic p=0.015).

We then measured social behaviour in adult *Cntnap2*$^{-/-}$ and *Cntnap2*$^{+/+}$ control mice in a male-female interaction test, and correlated the measured social scores with DMN hypoconnectivity measures. Consistent with previous reports (Penagarikano et al., 2011), behavioural testing revealed significantly impaired social interest (Fig. 4, A and B, left, total sniffing, p=0.030; social investigations, p=0.023) and increased non-social behaviour (Fig. S6, wall-rearing frequency, p=0.005) in *Cntnap2*$^{-/-}$ mutants compared to *Cntnap2*$^{+/+}$ control littermates. Hypoconnectivity in key DMN components (retrosplenial-cingulate cortex) was significantly associated with reduced social behaviour (Fig 4, A and B, right, p=0.034 and p=0.040, respectively) and increased non-social behaviour (Fig. S6 B, p=0.020). These findings highlight a correlation between fronto-posterior connectivity and social behaviour, suggesting that impaired functional couplings

produced by mutations in CNTNAP2 could reverberate to affect complex behavioural traits such as sociability and social exploration.

Macroscale cortico-cortical white matter connectivity is preserved in Cntnap2$^{-/-}$ mice

To further probe a role of macroscale anatomical connectivity on the observed functional decoupling in *Cntnap2*$^{-/-}$, we performed tractography analysis of the corpus callosum and cingulum, two major white matter tracts characterised by extensive cortico-cortical antero-posterior extension. These white matter tracts appeared to be largely typical in mutant and control mice as seen with ROI-based tractography (Fig. 5). In keeping with this, we did not observe statistically significant differences in the number of streamlines between *Cntnap2*$^{-/-}$ mutants and controls ($p = 0.21$ and $p = 0.25$, for cingulum and corpus callosum, respectively, Fig S7). These results suggest that the observed functional connectivity changes do not reflect major macroscale alterations in white matter wiring, but are likely to reflect functional desynchronization between involved regional substrates.

Discussion

Here we show that homozygous mice lacking CNTNAP2, a neurexin superfamily member associated with autism, exhibit reduced long-range and local functional connectivity in prefrontal cortical regions and midline functional hubs of the mouse brain. We also show that reduced fronto-posterior connectivity is associated with impaired social behaviour, revealing a possible link between long-range functional connectivity alterations and mouse behavioural traits recapitulating ASD symptoms. Collectively, these findings suggest that loss-of-function mutations in CNTNAP2 may predispose to neurodevelopmental disorders and autism through dysregulation of macroscale functional network couplings.

Our use of an imaging readout widely employed in human connectivity mapping provides us with the opportunity to cross-compare connectivity findings across species. In this respect, the observation of long-range fronto-posterior hypo-connectivity in Cntnap2$^{-/-}$ mice is especially noteworthy, because it is in excellent agreement with the results of a recent human imaging study where an association between common genetic variants in CNTNAP2 and similar long-range frontal hypoconnectivity was described (Scott-Van Zeeland et al., 2010). Our results expand these findings, by revealing a causal contribution of Cntnap2 loss-of-function mutations to long-range fronto-cortical connectivity impairments. These correspondences also serve as an important proof-of-concept demonstration that ASD-related genetic mutations can lead to comparable macroscale connectivity deficits in humans and lower mammal species like the laboratory mouse. The presence of long-range hypoconnectivity in Cntnap2$^{-/-}$ mice also adds to the remarkable construct and face validity of this mouse model as an experimental tool for

mechanistic and therapeutic investigation of syndromic forms of ASD (Penagarikano et al., 2011). Specifically, Cntnap2$^{-/-}$ mice closely phenocopy many major neuropathological features observed in cortical dysplasia-focal epilepsy (CDFE) syndrome, a rare neuronal migration disorder associated with a recessive (suggesting loss of function) mutation in CNTNAP2, and, in nearly two thirds of patients, with autism (Strauss et al., 2006). These include behavioural deficits in the three core domains of ASD (reduced vocal communication, repetitive and restricted behaviours, and abnormal social interactions), hyperactivity and epileptic seizures (both features described in CDFE patients), and reduced GABAergic interneurons, resulting in asynchronous cortical activity as measured with in vivo two-photon calcium imaging (Penagarikano et al., 2011).

A role of GABA-mediated impairments in brain synchronization represents a plausible mechanistic correlate of the impaired functional decoupling described in the present work, given the key contribution of GABAergic oscillatory rhythm in mediating large-scale functional synchrony (Gonzalez-Burgos and Lewis, 2008). However, our limited understanding of the cellular and neurobiological cascade leading to large scale functional connectivity abnormalities does not permit to provide a clear mechanistic explanation for the presence of regional, rather than widespread, alterations in functional desynchronizations. The observation of largely conserved macroscale white matter organization in Cntnap2$^{-/-}$ mice argue against the observed functional decoupling being the direct consequence of macroscopic anatomical rewiring. Regional differences in GABAergic interneuron density, or developmental processes related to circuit and network refinements (Zhan et al., 2014;Riccomagno and Kolodkin, 2015) could more plausibly play a role in the development of the observed regional desynchronization, an

hypothesis consistent with recent evidence of altered spine density and increase spine eliminations in Cntnap2$^{-/-}$ mice (Gdalyahu et al., 2015).

The observation of hypoconnectivity in prefrontal hub regions of the DMN (Liska et al., 2015) is suggestive of a deficient "maturation" of this functional network (Supekar et al., 2010), and is in keeping with the hypothesis of a key role of this region as a mediator of deficits in global perception and its cognitive representations in ASD patents (Martinez-Sanchis, 2014). The notion that "underconnectivity" may preferentially affect complex cognitive and social functions and their high order cortical substrates rather than low-level sensory and perceptual tasks has recently found some theoretical support (Kana et al., 2011). Within this framework, heteromodal integrative hubs like the anterior cingulate and prefrontal cortex, as well as retrosplenial regions would serve as major points of vulnerability for the stability of distributed functional networks couplings. rsfMRI mapping in additional mouse lines harbouring ASD-related genetic mutations will be instrumental in assessing whether the observed alterations represent a generalizable endophenotype that may converge across mutations and genetic etiologies, or are the specific consequence of CNTNAP2 mutations. It is however interesting to note that so far hypo-connectivity appears to be predominant in mouse imaging studies of ASD: reduced connectivity in several brain regions including the prefrontal cortex and the DMN has been observed in the BTBR model of idiopathic autism (Sforazzini et al., 2014a), and in mice characterised by reduced synaptic pruning (Zhan et al., 2014), a pathological trait associated with autism (Tang et al., 2014). Reduced connectivity between motor sensory regions was also recently described in a mouse model of fragile X syndrome (Haberl et al., 2015). Although preliminary, these initial mouse findings are consistent with and somehow support the "under-connectivity theory" of

autism, according to which reduced functional connectivity (at least in the adult brain (Uddin et al., 2013)) may emerge as a dominant feature of ASD in the face of heterogeneous etiopathological path-ways (Di Martino et al., 2013;Uddin et al., 2013).

In contrast with our imaging results, human rsfMRI mapping in CNTNAP2 common variant carriers revealed increased, instead of decreased, local connectivity in lateral prefrontal regions. The reason behind this discrepancy is not clear, although several important experimental factors, including methodological, species- or age-related differences may contribute to this inconsistency. For example, local connectivity increase in humans was observed in lateral prefrontal areas, a region that does not have a clear cyto-architectural correlate in rodents (Vogt and Paxinos, 2014). Moreover, our study was performed in adult subjects, while human mapping was carried out in children. The investigation of the neurodevelopmental trajectory of these alterations may help clarify this inconsistency. Differences in the nature of the investigated mutations should also not be neglected, as the functional consequences of the genetic variants imaged by Van Zeeland et al., (Scott-Van Zeeland et al., 2010) are unclear, and the possibility that not all the genetic variants imaged are loss-of-function cannot be ruled out.

In conclusion, we document that absence of CNTNAP2 leads to local and long-range connectivity reductions in prefrontal functional hubs of the mouse brain, an effect associated with impaired social behaviour. The lack of white-matter connectional alterations at the macroscale level suggests that the observed functional connectivity alterations reflect functional decoupling, rather than major anatomical re-wiring. Collectively, these findings suggest that loss-of-function mutations in CNTNAP2 may predispose to neurodevelopmental disorders and autism through

dysregulation of macroscale functional network couplings, and provide a translational model for investigating connectional perturbations in syndromic ASD forms.

Acknowledgments

The study was funded by a grant from the Simons Foundation (SFARI 314688, A.G.).

Conflict of interests

The authors declare that they have no conflict of interest.

Figures

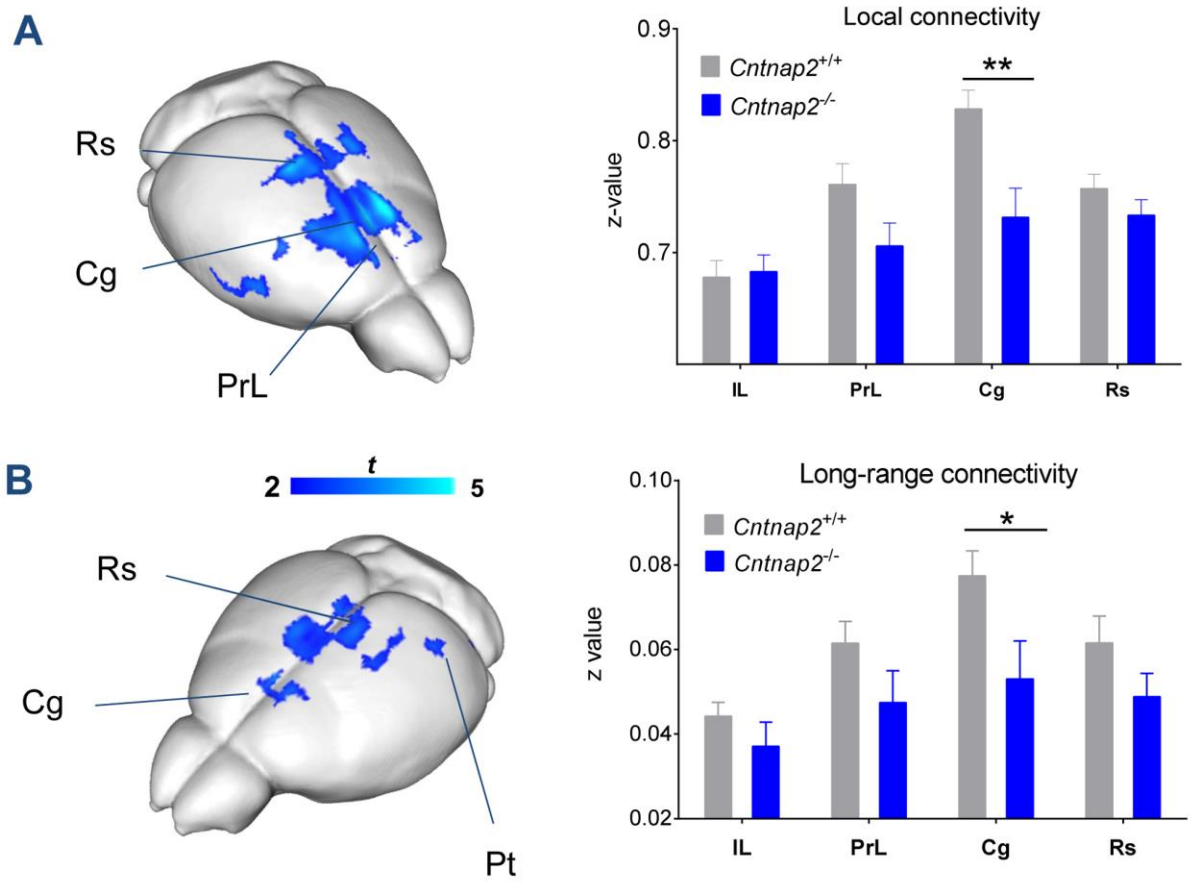

Figure 1

Reduced local (A) and long-range (B) connectivity in Cntnap2$^{-/-}$ mutants. Blue indicates statistically significant reduced connectivity in C*ntnap2*$^{-/-}$ vs. control C*ntnap2*$^{+/+}$ littermates (left, $p < 0.05$, cluster corrected). The effect was also separately quantified in anatomical volumes of interest (right IL: infra-limbic cortex; PrL: prelimbic cortex, Cg: Cingulate Cortex; Rs: retrosplenial cortex). * $p< 0.05$, **$p< 0.01$. Local connectivity difference in the prelimbic cortical volume was also close to significance ($p=0.053$).

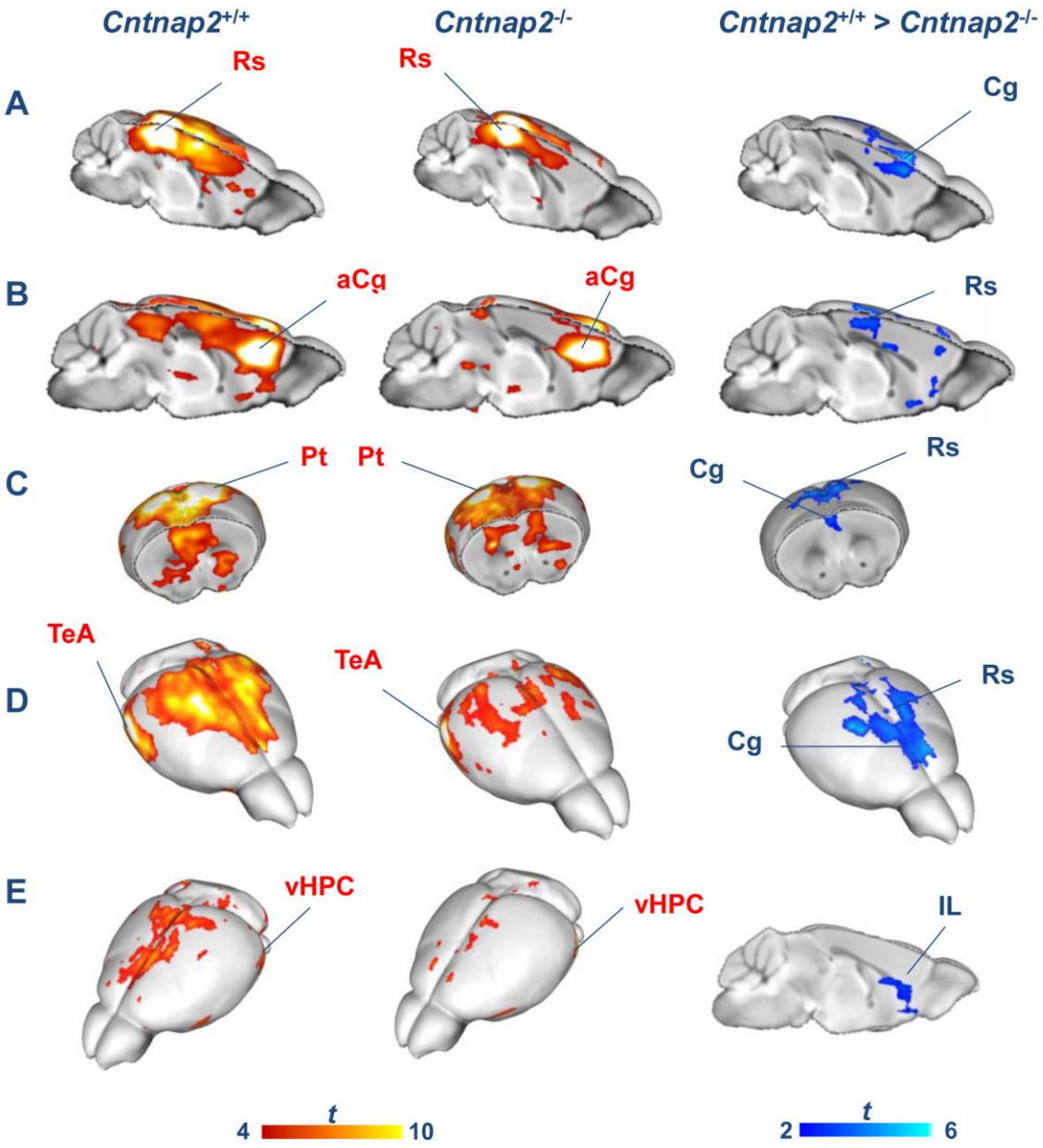

Figure 2

Reduced long-range connectivity in Cntnap2$^{-/-}$ mice. Seed-correlation mapping highlighted convergent reduced connectivity between long-range cortical and subcortical regions and cingulate-prefrontal areas. Red/yellow indicates significant correlation with seed regions (in red,

$p < 0.05$, cluster corrected). Blue indicates foci of reduced connectivity in *Cntnap2*$^{-/-}$ mutants ($p < 0.05$, cluster corrected) with respect to control mice. Rs: retrosplenial cortex, IL: infra-limbic cortex; aCg: anterior cingulate cortex, Cg: cingulate Cortex; Rs: retrosplenial cortex, vHPC: ventral hippocampus, Au/TeA: auditory/temporal associated cortices, Pt: parietal cortex.

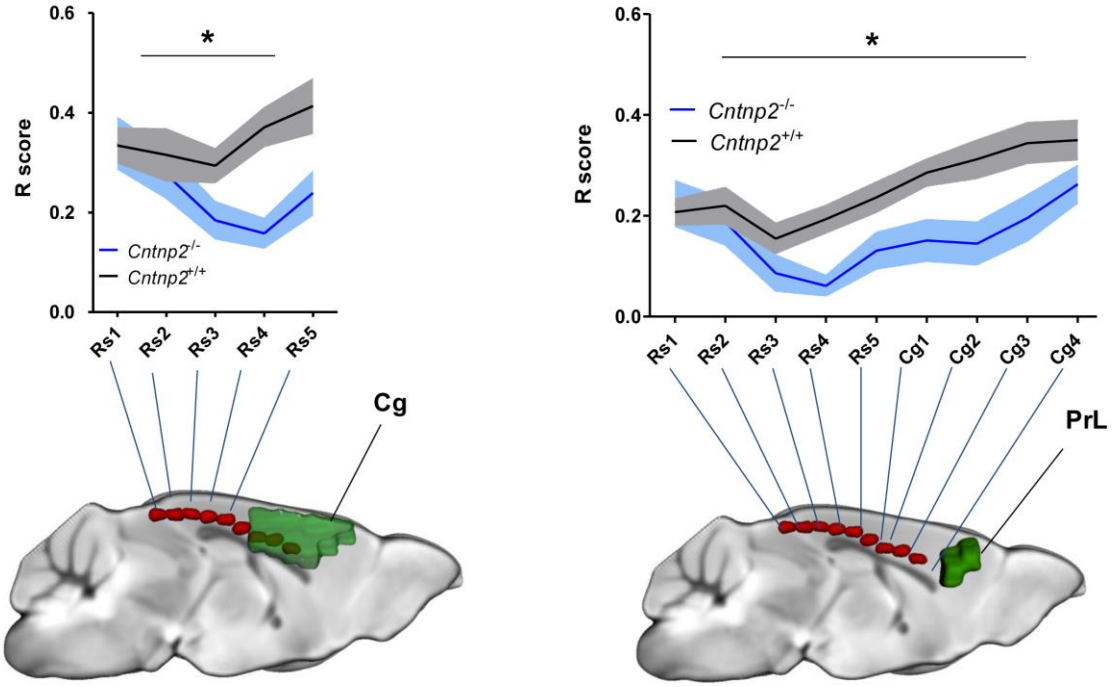

Figure 3

Fronto-posterior hypoconnectivity in *Cntnap2*$^{-/-}$ mice. Reduced long-range connectivity in midline regions of the DMN in *Cntnap2*$^{-/-}$ mice. Connectivity profile between retrosplenial (Rs) seeds (red) and the cingulate cortex (Cg VOI, green, left), and between retrosplenial/cingulate seeds (red) and the prelimbic cortex (PrL VOI, green, right). *p<0.05, genotype effect, 2-way ANOVA .

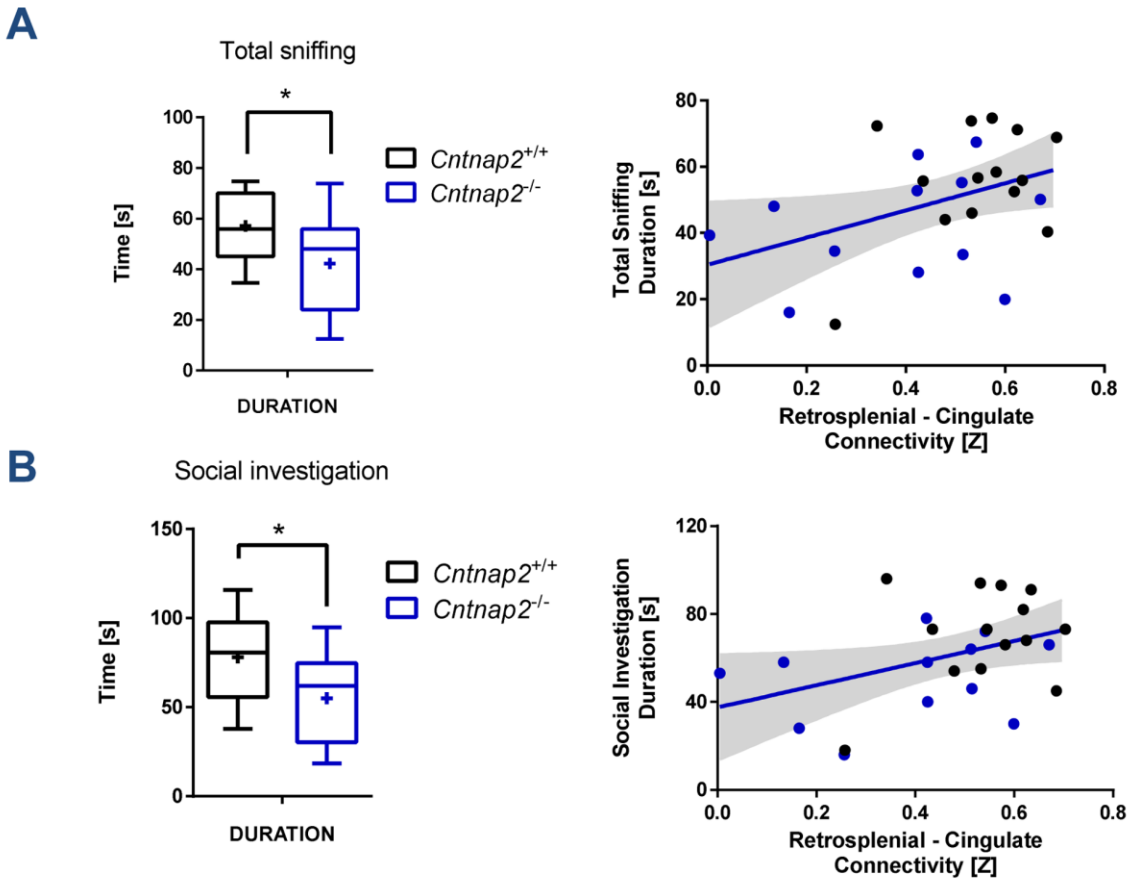

Figure 4

Fronto-posterior connectivity was inversely correlated with social behaviour. *Cntnap2*$^{-/-}$ mice exhibited reduced social behaviour (A, total sniffing, p=0.030; B, social investigation, p=0.023). Connectivity between retrosplenial and cingulate cortices (VOI to VOI) was found to be associated with social behaviour (A, total sniffing, p=0.034; B, social investigation, p=0.040).

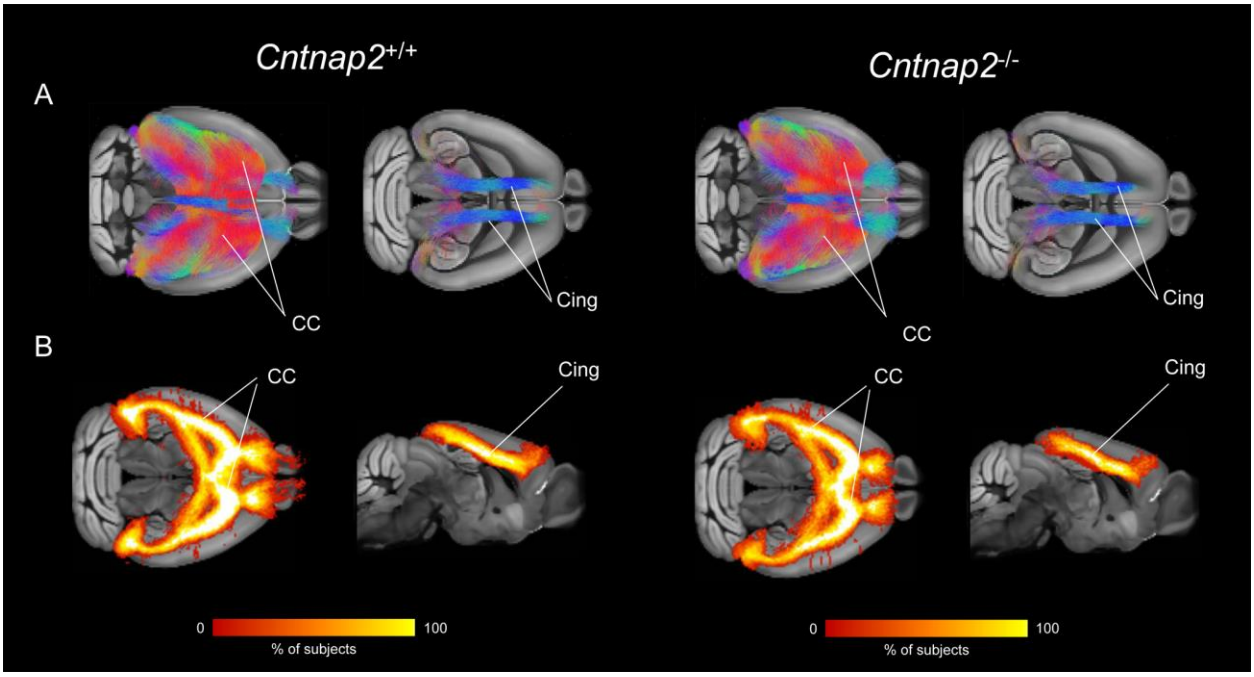

Figure 5

Preserved cortico-cortical white matter organization in *Cntnap2*$^{-/-}$ mutants. (A) Corpus callosum and cingulum tracts virtually dissected in two representative subjects (*Cntnap2*$^{+/+}$ left, *Cntnap2*$^{-/-}$ right), (B) Fractional group fibre density maps for corpus callosum and cingulum tracts (*Cntnap2*$^{+/+}$ left, *Cntnap2*$^{-/-}$, right).

Reference List

Alarcin M, Abrahams BS, Stone JL, Duvall JA, Perederiy JV, Bomar JM, Sebat J, Wigler M, Martin CL, Ledbetter DH (2008) Linkage, association, and gene-expression analyses identify CNTNAP2 as an autism-susceptibility gene. The American Journal of Human Genetics 82:150-159.

Anagnostou E, Taylor M (2011) Review of neuroimaging in autism spectrum disorders: what have we learned and where we go from here. Molecular Autism 2:4.

Auerbach BD, Osterweil EK, Bear MF (2011) Mutations causing syndromic autism define an axis of synaptic pathophysiology. Nature 480:63-68.

Buckner RL, Sepulcre J, Talukdar T, Krienen FM, Liu HS, Hedden T, Andrews-Hanna JR, Sperling RA, Johnson KA (2009) Cortical Hubs Revealed by Intrinsic Functional Connectivity: Mapping, Assessment of Stability, and Relation to Alzheimer's Disease. J Neurosci 29:1860-1873.

Cole MW, Anticevic A, Repovs G, Barch D Variable Global Dysconnectivity and Individual Differences in Schizophrenia. Biological Psychiatry 70:43-50.

Cole MW, Pathak S, Schneider W (2010) Identifying the brain's most globally connected regions. NeuroImage 49:3132-3148.

Di Martino A, et al. (2013) The autism brain imaging data exchange: towards a large-scale evaluation of the intrinsic brain architecture in autism. Mol Psychiatry.

Dodero L, Damiano M, Galbusera A, Bifone A, Tsaftsaris SA, Scattoni ML, Gozzi A (2013) Neuroimaging Evidence of Major Morpho-Anatomical and Functional Abnormalities in the BTBR T+TF/J Mouse Model of Autism. PLoS ONE 8:e76655.

Ferrari L, Turrini G, Crestan V, Bertani S, Cristofori P, Bifone A, Gozzi A (2012) A robust experimental protocol for pharmacological fMRI in rats and mice. Journal of Neuroscience Methods 204:9-18.

Garyfallidis E, Brett M, Amirbekian B, Rokem A, Van Der Walt S, Descoteaux M, Nimmo-Smith I (2014) Dipy, a library for the analysis of diffusion MRI data. Frontiers in Neuroinformatics 8.

Gdalyahu A, Lazaro M, Penagarikano O, Golshani P, Trachtenberg JT, Geschwind DH (2015) Correction: The Autism Related Protein Contactin-Associated Protein-Like 2 (CNTNAP2) Stabilizes New Spines: An <italic>In Vivo</italic> Mouse Study. PLoS ONE 10:e0129638.

Gonzalez-Burgos G, Lewis DA (2008) GABA Neurons and the Mechanisms of Network Oscillations: Implications for Understanding Cortical Dysfunction in Schizophrenia. Schizophr Bull 34:944-961.

Gozzi A, Schwarz AJ (2015) Large-scale functional connectivity networks in the rodent brain. NeuroImage.

Haberl MG, Zerbi V, Veltien A, Ginger M, Heerschap A, Frick A (2015) Structural-functional connectivity deficits of neocortical circuits in the Fmr1Γêǽ/y mouse model of autism. Science advances 1:e1500775.

Just MA, Keller TA, Malave VL, Kana RK, Varma S (2012) Autism as a neural systems disorder: A theory of frontal-posterior underconnectivity. Neuroscience & Biobehavioral Reviews 36:1292-1313.

Kana RK, Libero LE, Moore MS (2011) Disrupted cortical connectivity theory as an explanatory model for autism spectrum disorders. Physics of Life Reviews 8:410-437.

Liska A, Galbusera A, Schwarz AJ, Gozzi A (2015) Functional connectivity hubs of the mouse brain. NeuroImage 115:281-291.

Liu X, Zhu XH, Zhang Y, Chen W (2011) Neural origin of spontaneous hemodynamic fluctuations in rats under burst-suppression anesthesia condition. Cereb Cortex 21:374-384.

Martinez-Sanchis S (2014) Neurobiological foundations of multisensory processing integration in people with autism spectrum disorders: The role of the medial prefrontal cortex. Frontiers in human neuroscience 8.

Nasrallah FA, Tay HC, Chuang KH (2014) Detection of functional connectivity in the resting mouse brain. NeuroImage 1:417-424.

Oguz I, Zhang H, Rumple A, Sonka M (2014) RATS: Rapid Automatic Tissue Segmentation in rodent brain MRI. Journal of Neuroscience Methods 221:175-182.

Paxinos G, Franklin K (2003) The Mouse Brain in Stereotaxic Coordinates. Sydney: Academic Press.

Penagarikano O, Abrahams B, Herman E, Winden K, Gdalyahu A, Dong H, Sonnenblick L, Gruver R, Almajano J, Bragin A, Golshani P, Trachtenberg J, Peles E, Geschwind D (2011) Absence of CNTNAP2 Leads to Epilepsy, Neuronal Migration Abnormalities, and Core Autism-Related Deficits. Cell 147:235-246.

Rane P, Cochran D, Hodge SM, Haselgrove C, Kennedy DN, Frazier JA (2015) Connectivity in autism: A review of MRI connectivity studies. Harvard review of psychiatry 23:223-244.

Riccomagno MM, Kolodkin AL (2015) Sculpting Neural Circuits by Axon and Dendrite Pruning. Annual Review of Cell and Developmental Biology 31:779-805.

Rodenas-Cuadrado P, Ho J, Vernes SC (2014) Shining a light on CNTNAP2: complex functions to complex disorders. European Journal of Human Genetics 22:171-178.

Sanders S, et al. (2015) Insights into Autism Spectrum Disorder Genomic Architecture and Biology from 71 Risk Loci. Neuron 87:1215-1233.

Scattoni ML, Gandhy SU, Ricceri L, Crawley JN (2008) Unusual repertoire of vocalizations in the BTBR T+tf/J mouse model of autism. PLoS ONE 3:e3067.

Scattoni ML, Martire A, Cartocci G, Ferrante A, Ricceri L (2013) Reduced social interaction, behavioural flexibility and BDNF signalling in the BTBR T+tf/J strain, a mouse model of autism. Behavioural Brain Research 251:35-40.

Scattoni ML, Ricceri L, Crawley JN (2011) Unusual repertoire of vocalizations in adult BTBR T+tf/J mice during three types of social encounters. Genes, Brain and Behavior 10:44-56.

Schreiner MJ, Karlsgodt KH, Uddin LQ, Chow C, Congdon E, Jalbrzikowski M, Bearden CE (2014) Default mode network connectivity and reciprocal social behavior in 22q11.2 deletion syndrome. Social Cognitive and Affective Neuroscience 9:1261-1267.

Scott-Van Zeeland AA, Abrahams BS, Alvarez-Retuerto AI, Sonnenblick LI, Rudie JD, Ghahremani D, Mumford JA, Poldrack RA, Dapretto M, Geschwind DH, Bookheimer SY (2010) Altered Functional Connectivity in Frontal Lobe Circuits Is Associated with Variation in the Autism Risk Gene CNTNAP2. Science Translational Medicine 2:56ra80.

Sforazzini F, Bertero A, Dodero L, David G, Galbusera A, Scattoni M, Pasqualetti M, Gozzi A (2014a) Altered functional connectivity networks in acallosal and socially impaired BTBR mice. Brain Struct Funct1-14.

Sforazzini F, Schwarz AJ, Galbusera A, Bifone A, Gozzi A (2014b) Distributed BOLD and CBV-weighted resting-state networks in the mouse brain. NeuroImage 87:403-415.

Steffey MA, Brosnan RJ, Steffey EP (2003) Assessment of halothane and sevoflurane anesthesia in spontaneously breathing rats. American Journal of Veterinary Research 64:470-474.

Strauss KA, Puffenberger EG, Huentelman MJ, Gottlieb S, Dobrin SE, Parod JM, Stephan DA, Morton DH (2006) Recessive symptomatic focal epilepsy and mutant contactin-associated protein-like 2. New England Journal of Medicine 354:1370-1377.

Supekar K, Uddin LQ, Prater K, Amin H, Greicius MD, Menon V (2010) Development of functional and structural connectivity within the default mode network in young children. NeuroImage 52:290-301.

Tang G, Gudsnuk K, Kuo SH, Cotrina M, Rosoklija G, Sosunov A, Sonders M, Kanter E, Castagna C, Yamamoto A, Yue Z, Arancio O, Peterson B, Champagne F, Dwork A, Goldman J, Sulzer D (2014) Loss of mTOR-Dependent Macroautophagy Causes Autistic-like Synaptic Pruning Deficits. Neuron 83:1131-1143.

Tournier JD, Calamante F, Connelly A (2007) Robust determination of the fibre orientation distribution in diffusion MRI: Non-negativity constrained super-resolved spherical deconvolution. NeuroImage 35:1459-1472.

Tournier JD, Calamante F, Connelly A (2012) MRtrix: Diffusion tractography in crossing fiber regions. Int J Imaging Syst Technol 22:53-66.

Uddin LQ, Supekar K, Menon V (2013) Reconceptualizing functional brain connectivity in autism from a developmental perspective. Frontiers in human neuroscience 7.

Vogt B, Paxinos G (2014) Cytoarchitecture of mouse and rat cingulate cortex with human homologies. Brain Struct Funct 219:185-192.

Yushkevich PA, Piven J, Hazlett HC, Smith RG, Ho S, Gee JC, Gerig G (2006) User-guided 3D active contour segmentation of anatomical structures: Significantly improved efficiency and reliability. NeuroImage 31:1116-1128.

Zhan Y, Paolicelli R, Sforazzini F, Weinhard L, Bolasco G, Pagani F, Vissosktsy A, Bifone A, Gozzi A, Ragozzino D, Gross C (2014) Deficient neuron-microglia signaling results in impaired functional brain connectivity and social behavior. Nat Neurosci 17:400-406.

Supplementary figures

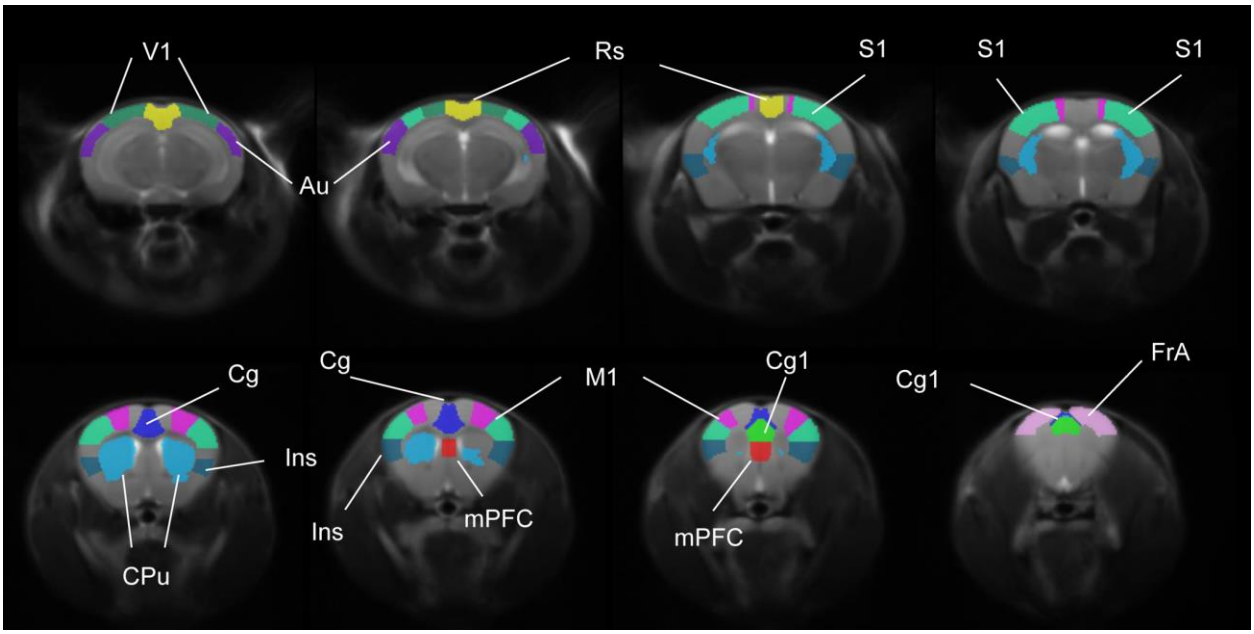

Figure S1

Volumes of interest used in functional connectivity mappings. V1: primary visual cortex, Au: auditory cortex, Rs: retrosplenial cortex, S1: primary somatosensory cortex, Cg: cingulate cortex, CPu: caudate-putamen, Ins: insular cortex, mPFC: medial prefrontal cortex, M1: primary motor cortex, Cg1: cingulate cortex, area 1, FrA: frontal association cortex

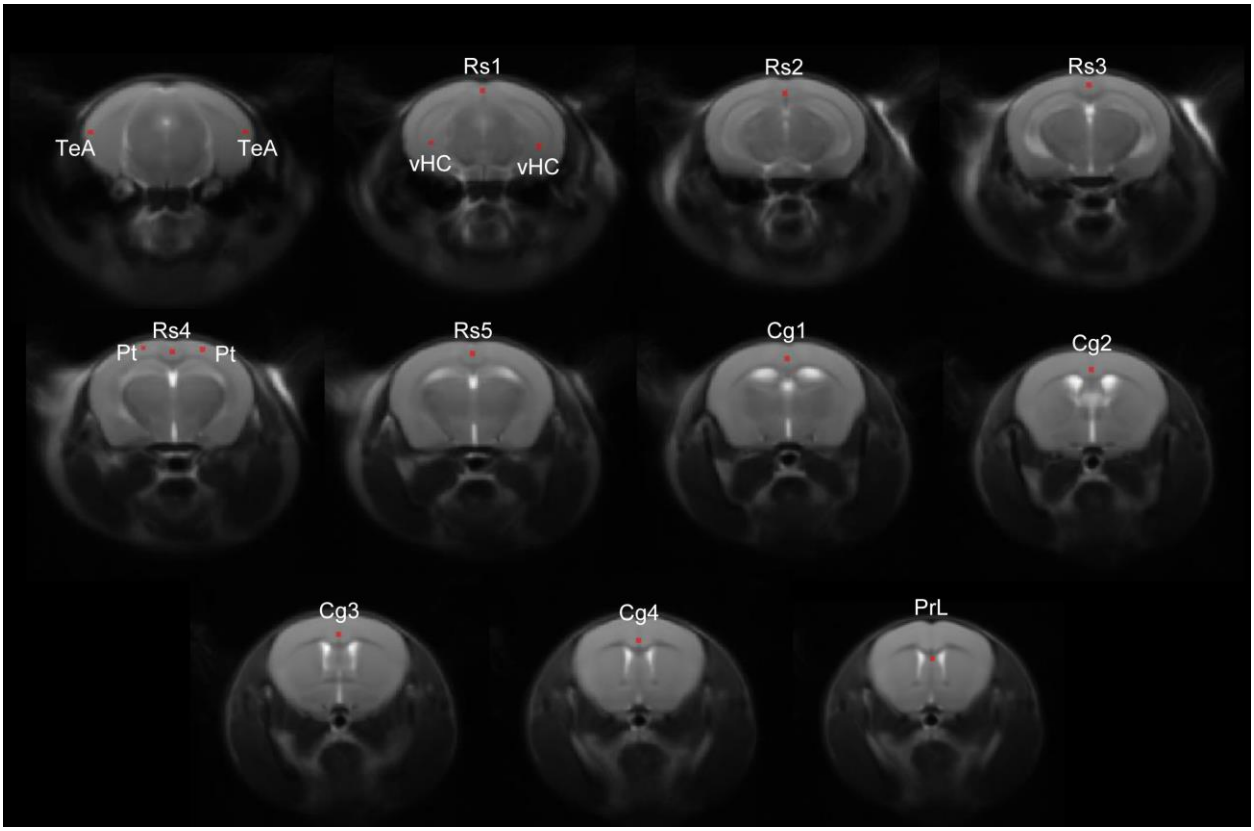

Figure S2

Location of seeds used in mapping anteroposterior DMN connectivity. TeA: temporal association cortex (bilateral), Rs: retrosplenial cortex, Cg: cingulate cortex, Pt: posterior parietal association cortex (bilateral), PrL: prelimbic cortex, vHC: ventral hippocampus.

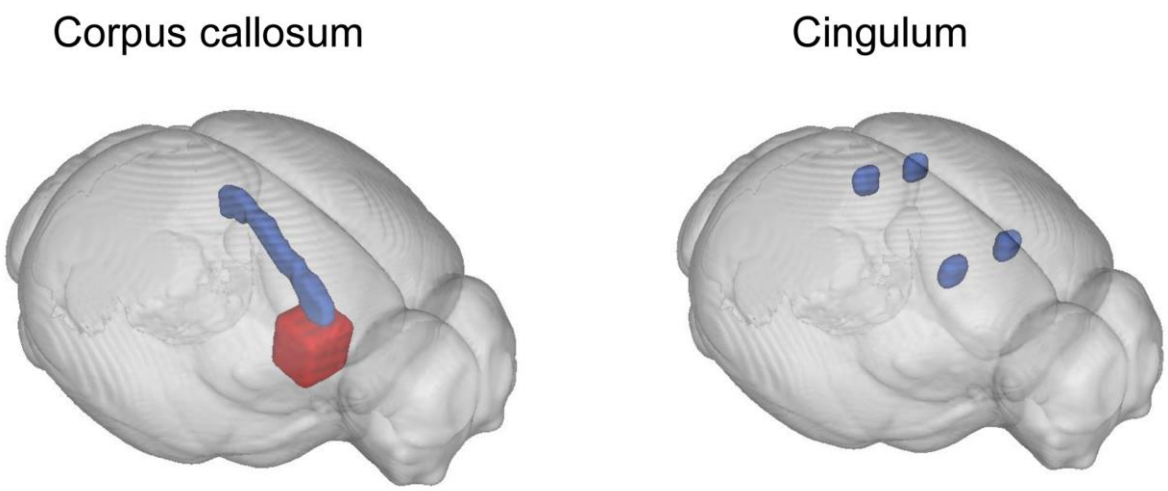

Figure S3

Location of waypoint ROIs used for virtual dissection of corpus callosum and cingulum tracts from whole-brain white matter tractography. Inclusion ROIs are indicated in blue, exclusion ROIs are indicated in red.

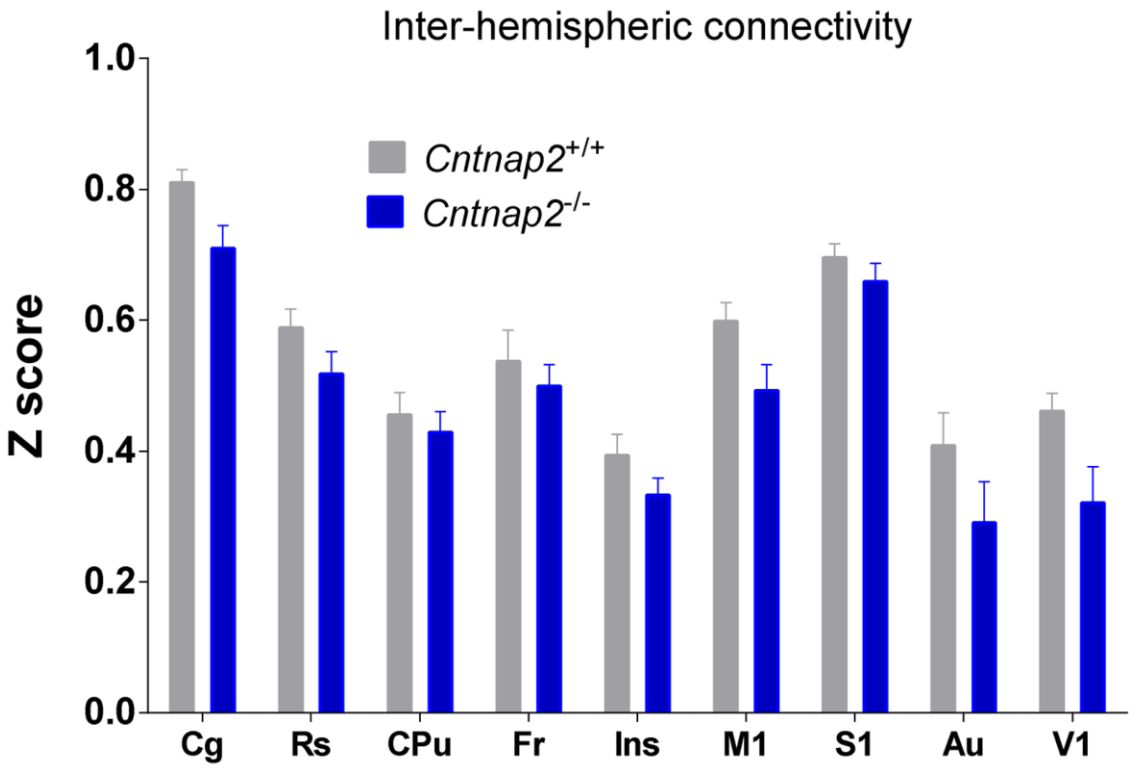

Figure S4

Largely preserved inter-hemispheric connectivity in *Cntnap2*$^{-/-}$ mutants and control mice. Correlation coefficients were calculated between time courses extracted from VOIs depicted in Fig. S1 and the resulting *r*-scores were transformed to *z*-scores using Fisher's *r*-to-*z* transform. None of these comparisons survived a false discover rate correction at q=0.05.

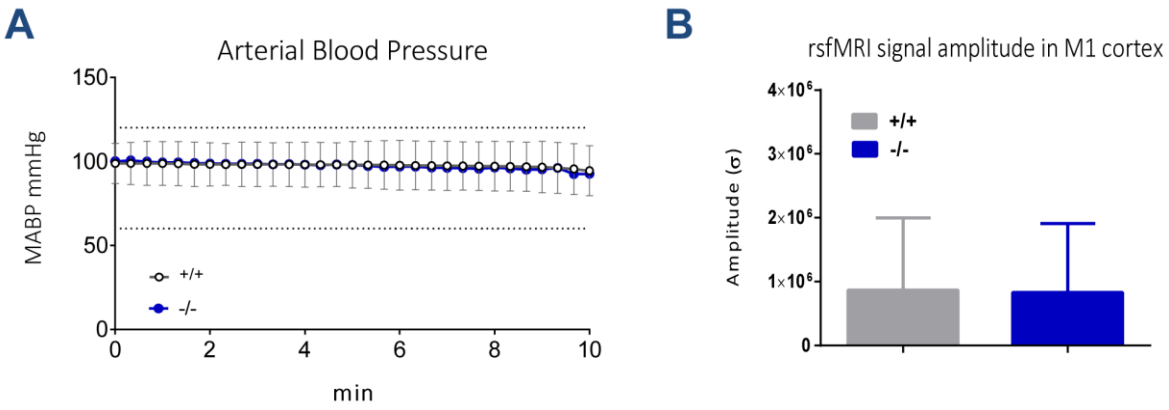

Figure S5

No genotype-dependent differences in anaesthesia sensitivity were detected as seen with mean arterial blood pressure mapping (A, p = 0.78) and amplitude of cortical BOLD signal fluctuations in primary motor cortex (B, p = 0.36). M1: primary motor cortex.

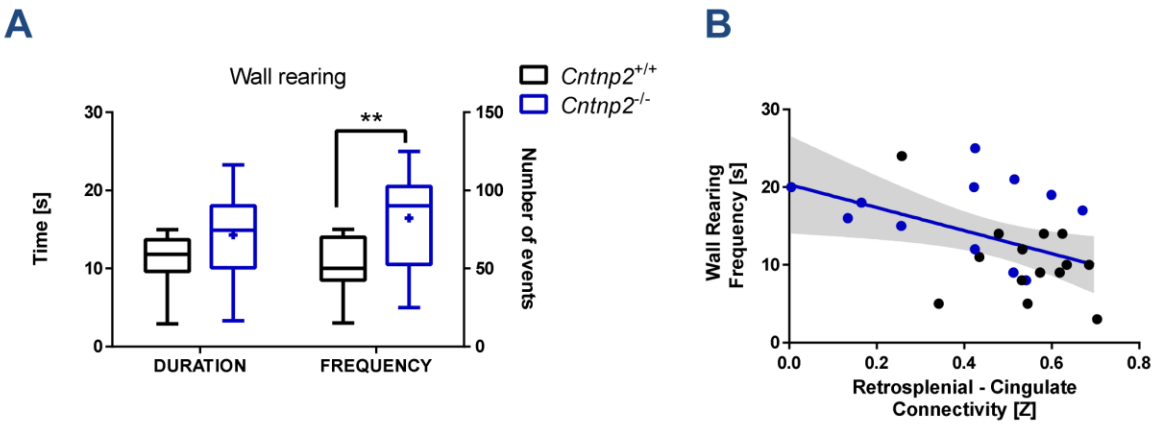

Figure S6

Increased non-social behaviour in *Cntnap2*$^{-/-}$ mutants compared to control littermates. (A) Non-social behaviour as measured by the time and frequency of rearing up against the wall of the home-cage (p=0.005). (B) An inverse association between non-social behaviour and connectivity between retrosplenial and cingulate cortices (p=0.020).

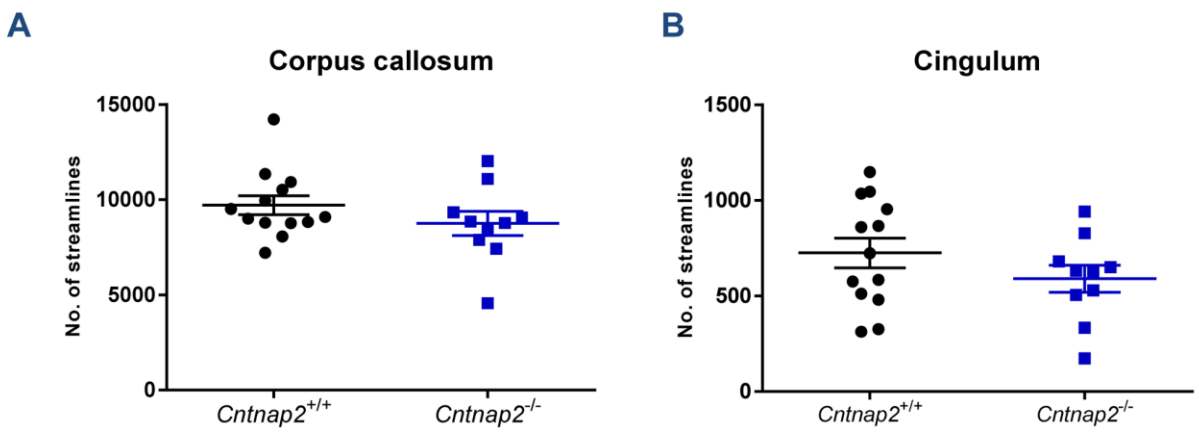

Figure S7

White-matter streamlines in *Cntnap2*$^{-/-}$ mutants compared to control littermates as estimated with DTI. No significant difference was observed in the number of streamlines generated by white-matter tractography in *Cntnap2*$^{-/-}$ mutants and controls for corpus callosum (A, p = 0.25) and cingulum (B, p = 0.21) tracts.